1 **Dynamic response and breakage of trees subject to a landslide-induced air blast**

2 Yu Zhuang[1,2], Aiguo Xing[1], Perry Bartelt[3], Muhammad Bilal[1], Zhaowei Ding[2]

3 [1]State Key Laboratory of Ocean Engineering, Shanghai Jiao Tong University, Shanghai, 200240, PR China

4 [2]State Key Laboratory of Geohazard Prevention and Geoenvironment Protection, Chengdu University of

5 Technology, Chengdu, 610059, China

6 [3]WSL Institute for Snow and Avalanche Research SLF, Flüelastrasse 11, 7260 Davos Dorf, Switzerland

7 Correspondence: Aiguo Xing (xingaiguo@sjtu.edu.cn)

9 **Abstract**

10 Landslides have been known to generate powerful air blasts capable of causing destruction and casualties

11 far beyond the runout of sliding mass. The extent of tree damage provides valuable information on air

12 blast intensity and impact region. However, little attention has been paid to the air blast-tree interaction.

13 In this study, we proposed a framework to assess the tree destruction caused by powerful air blasts,

14 including the eigenfrequency prediction method, tree motion equations and the breakage conditions. The

15 tree is modeled as a flexible beam with variable cross-sections, and the anchorage stiffness is introduced

16 to describe the tilt of tree base. Large tree deflection is regarded when calculating the air blast loading,

17 and two failure modes (bending and overturning) and the associated failure criteria are defined. Modeling

18 results indicate that although the anchorage properties are of importance to the tree eigenfrequency, tree

19 eigenfrequency is always close to the air blast frequency, causing a dynamic magnification effect for the

20 tree deformation. This magnification effect is significant in cases with a low air blast velocity, while the

21 large tree deflection caused by strong air blast loading would weaken this effect. Furthermore, failure

22 modes of a specific forest subject to a powerful air blast depend heavily on the trunk bending strength

23   and anchorage characteristics. The large variation of biometric and mechanical properties of trees

24   necessitates the establishment of a regional database of tree parameters. Our work and the proposed

25   method are expected to make people better understand air blast power and be of great utility for air blast

26   risk assessment in mountainous regions worldwide.

27   **Keywords:** Landslide-induced air blast; Tree eigenfrequency; Dynamic response; Tree breakage

28   **1 Introduction**

29   Long runout landslides involve massive amounts of energy and can be extremely hazardous owing to

30   their long movement distance, high mobility and potential chain disasters (Nicoletti and Sorriso Valvo,

31   1991; Nicoletti et al., 1993; Johnson and Campbell, 2017; Shugar et al., 2021; Zhang et al., 2022). A

32   moving landslide with high velocity can generate a powerful air blast capable of uprooting trees, lifting

33   people into the air and even flattening buildings (Adams, 1881; Penna et al., 2021). In recent decades,

34   destructive air blasts frequently occurred in mountainous regions worldwide and caused casualties and

35   economic loss far beyond the landslide runout (e.g., Yin, 2014; Bartelt et al., 2016; Kargel et al., 2016).

36   Understanding their force of destruction is of great utility for landslide risk assessment and disaster

37   mitigation, especially in high-altitude regions.

38   Monitoring equipment has been confirmed to provide great performance in determining the dynamic

39   characteristics of landslide-induced air blasts (Grigoryan et al., 1982; Sukhanov, 1982; Caviezel et al.,

40   2021). However, most case histories occurred in the high-altitude mountainous region without witnesses

41   (Yin and Xing, 2012), and the in-situ equipment can also get damaged because of the near-field

42   destruction of landslides and associated air blasts. Therefore, very few air blast cases were measured in

43   history. Geologists can only evaluate the air blast hazard for most recorded events using historical

44   evidence after the landslide occurred. In-situ information about forest destruction and tree breakage is

45   often used for the air blast risk assessment (Feistl et al., 2015; Fujita et al., 2017; Zhuang et al., 2019,

46   2022a) (Fig. 1). Uprooted trees and snapped stems delineate the impact region of air blasts and create a

47   natural vector field indicating the primary movement direction of the landslide, greatly helping analyze

48   the disaster-causing process of the event. In many cases, observations of forest destruction are the only

49   data to quantify air blast danger.

50

51   **Fig. 1** Trees breakage caused by a large landslide-induced air blast in Sichuan, China, 2008.

52   A question remained for air blast mitigation planning using the information of tree damage is how

53   to establish a simple relationship between air blast impact pressure and tree failure. Bending and

54   overturning are two common tree failure modes caused by strong winds. Trees snap when the bending

55   stress exerted by the air blast exceeds the wood strength (Peltola et al., 1999; Gardiner et al., 2000), while

56   the overturning will occur if the applied moment overcomes the anchorage resistance of root systems

57   (Jonsson et al., 2006; Nicoll et al., 2006). The occurrence of these two failure modes depends heavily on

58   both the air blast loading and tree properties. Considering the minor destruction of air blasts relative to

59   the landslide, although long recognized that sliding mass can easily break or uproot trees (Bartelt and

60   Stöckli, 2001; Šilhán, 2020), little attention has been paid to the tree destruction resulting from air blasts.

61   Furthermore, existing models describing the tree-air blast interaction are mostly static (Feistl et al., 2015)

62   or established based on the small-deflection theory (Bartelt et al., 2018). These methods could aid in a

63   rapid assessment of air blast power, but further research is needed to establish a dynamic model to

64   represent the dynamic response of trees in a strong wind. A mechanical understanding of how trees are

65   damaged by air blasts is therefore essential for quantifying the air blast powers and providing valuable

66   data to verify the possible numerical results.

67   In this study, we established a simple dynamic model capable of calculating the natural frequency

68   of trees and simulating their dynamic response subject to a powerful air blast. The proposed model

69   regards the tree as a multi-degree-of-freedom beam with variable diameters and accounts for large tree

70   deflections and impacts of root anchorage. Both bending and overturning failure modes are involved in

71   the model. The work conducted in this study is expected to make people better understand the power of

72   landslide-induced air blasts and provide an applicable method to assess the air blast hazard.

73   **2. Model description**

74   Measurements of historical events indicated that the landslide-induced air blast is intermittent and of

75   short duration, lasting only a few seconds and could reach a high velocity (Grigoryan et al., 1982;

76   Sukhanov, 1982; Caviezel et al., 2021). This impulse wave has a propagation distance of hundreds of

77   meters in both horizontal and vertical directions and acts over the entire tree. Thus, the impact of air

78   blasts on trees is similar to extreme wind gusts, producing large bending moments in the stem and root

79   base system, forcing trees to deform or get damaged. Furthermore, fallen trees often point to the

80   movement direction of the landslide, illustrating there is little time for trees to sway and react to air blasts

81   while the inertial effects are greatly important.

82   To characterize the dynamic response of trees under the impact load of air blasts, we established a

83   mechanical model to predict the eigenfrequency of trees subject to air blasts and developed a dynamic

84   tree-swaying model that accounts for the large tree deflection. In what follows, we present the

85   eigenfrequency prediction method, tree motion equations and the breakage conditions.

86   *2.1 Eigenfrequency prediction*

87   The tree is modeled as a flexible cantilever beam with variable diameters that is hinged at ground level

88   using elastic support. The beam diameter is assumed to continuously linearly decrease with height

89   regarding the decreasing diameters of trunk and crown from bottom to top, while the anchorage stiffness

90   of the root system (K) helps to describe the tilt of tree base in response to the moment (Neild and Wood,

91   1999). In the eigenfrequency prediction mode, the tree beam is divided into two segments with a splitting

92   point located at the starting point of the tree crown (Fig. 2). We assume that the tree crown shows minor

93   impacts on elastic modulus. The tree crown is accounted for through the crown mass, and thus the natural

94   difference between the two segments is the material density.

95   The governing differential equation for the dynamic bending of a nonuniform Euler-Bernoulli beam

96   is (Keshmiri et al., 2018):

97
$$\rho A(z)\frac{\partial^2 u}{\partial t^2} + \frac{\partial^2 u}{\partial z^2}\left[EI(z)\frac{\partial^2 u}{\partial z^2}\right] = 0 \tag{1}$$

98   where z is the position variable along the beam length. For ease of calculation, the original point ($z=0$) is

99   set at the treetop and the maximum value of z is at the tree base, so that the beam diameter $d(z)$

100   corresponding to the position z can be described using a gradient coefficient (μ): $d(z)=\mu z$. u is the beam

101   displacement, E is the elastic modulus, $A(z) = \frac{\pi}{4}(dz)^2$ and $I(z) = \frac{\pi}{64}(dz)^4$ are the cross-sectional area

102   and moment of inertia, respectively.

103
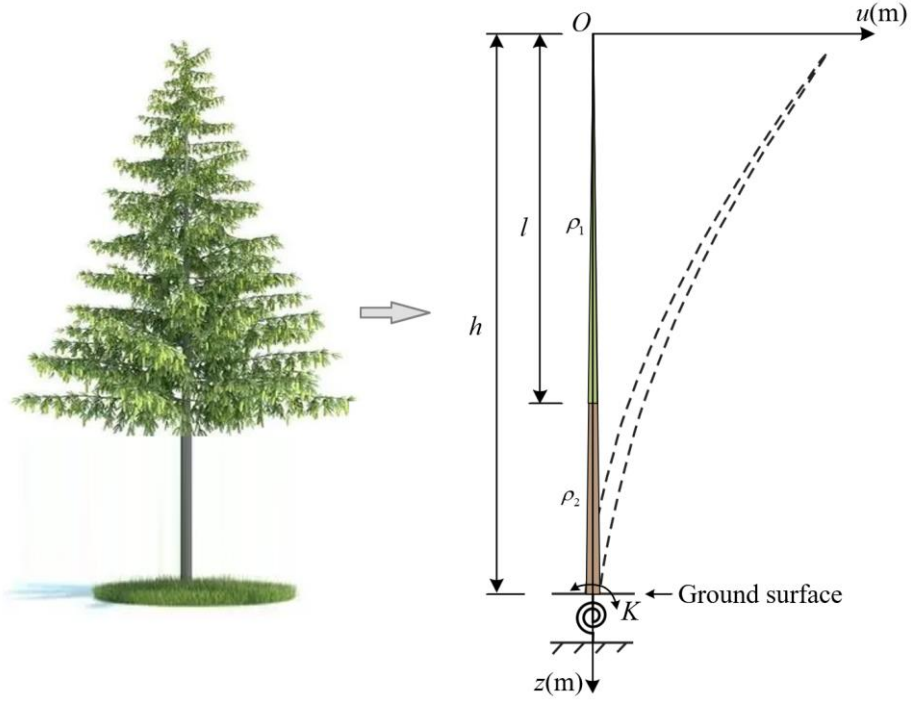
104   **Fig. 2** Schematic representation of the eigenfrequency prediction model.

105   Plugging the expression of $A(z)$ and $I(z)$ into Eq. 1 gives:

106
$$z^2 \frac{\partial^4 u}{\partial z^4} + 8z \frac{\partial^3 u}{\partial z^3} + 12 \frac{\partial^2 u}{\partial z^2} - \frac{16\rho\omega^2 u}{E\mu^2} = 0 \tag{2}$$

107   where ω is known as the eigenfrequency of the beam. The general solution of Eq. 2 can be expressed as:

108
$$u(z) = \frac{1}{z}\left[A_1 J_2(2\sqrt{\lambda z}) + A_2 Y_2(2\sqrt{\lambda z}) + A_3 J_2(2i\sqrt{\lambda z}) + A_4 Y_2(2i\sqrt{\lambda z}) \right] \tag{3}$$

109   where $\lambda = \sqrt{\dfrac{16\rho\omega^2}{E\mu^2}}$, J_2 and Y_2 are the Bessel functions of the first and second kind (Mocica, 1988),

110   respectively, and A_1-A_4 are coefficients that need to be determined based on the boundary conditions.

111   The deflection of the upper segment (crown) and the lower segment (trunk) can be generated in a

112   similar manner:

113
$$u_1(z) = \frac{1}{z}\left[A_1 J_2\left(2\sqrt{\lambda_1 z}\right) + A_2 Y_2\left(2\sqrt{\lambda_1 z}\right) + A_3 J_2\left(2i\sqrt{\lambda_1 z}\right) + A_4 Y_2\left(2i\sqrt{\lambda_1 z}\right) \right] \quad 0 \leqslant z < l \tag{4}$$

114
$$u_2(z) = \frac{1}{z}\left[B_1 J_2\left(2\sqrt{\lambda_2 z}\right) + B_2 Y_2\left(2\sqrt{\lambda_2 z}\right) + B_3 J_2\left(2i\sqrt{\lambda_2 z}\right) + B_4 Y_2\left(2i\sqrt{\lambda_2 z}\right) \right] \quad l \leqslant z \leqslant h \tag{5}$$

115   where l is the length of crown, h is the tree height, $\lambda_1 = \sqrt{\dfrac{16\rho_1\omega^2}{E\mu^2}}$ and $\lambda_2 = \sqrt{\dfrac{16\rho_2\omega^2}{E\mu^2}}$ are the single-valued

116   function of eigenfrequency. ρ_2 is the wood density and ρ_1 is the equivalent density regarding the

117   contribution of both tree trunk and crown. Same to A_1-A_4, B_1-B_4 are also coefficients of the tree deflection

118   equation that need to be determined based on the boundary and continuity conditions.

119   The boundary condition at the origin (z=0) is the free end, and thus Eq. 4 can be simplified as:

120
$$u_1(z) = \frac{1}{z}\left[A_1 J_2\left(2\sqrt{\lambda_1 z}\right) + A_3 J_2\left(2i\sqrt{\lambda_1 z}\right) \right] \quad 0 \leq z < l \qquad (6)$$

121   According to continuity conditions of two segments at the splitting point and the boundary condition

122   at the tree base, following constraints are determined: $u_1(l) = u_2(l)$, $u_1'(l) = u_2'(l)$, $u_1''(l) = u_2''(l)$,

123      $u_1'''(l) = u_2'''(l)$, $u_2(h) = 0$, and $Ku_2'(h) + EI(h)u_2''(h) = 0$. Introducing the constraints into Eqs. (5-6), a total

124   of six equations are determined here. These six equations can be written in a matrix format:

125
$$\left[F\left(\lambda_1, \lambda_2\right) \right]_{6\times 6} \cdot \left[A_1 \quad A_3 \quad B_1 \quad B_2 \quad B_3 \quad B_4 \right]^T = 0 \qquad (7)$$

126   where $\left[F\left(\lambda_1, \lambda_2\right) \right]_{6\times 6}$ is a matrix that is composed of λ_1 and λ_2. The orders of eigenfrequency and

127   the corresponding vibration mode can be obtained by solving the equation: the determinant of matric

128      $\left| F(\lambda_1, \lambda_2) \right| = 0$. Notably, the derivatives of $u_1(z)$ and $u_2(z)$ have very complicated expressions but could

129   be easily calculated using Matlab. Therefore, we did not provide the complete expression here.

130   *2.2 Tree motion*

131   The mechanical response of trees subject to an air blast is modeled using a modified multi-degree-of-

132   freedom tree swaying model with variable cross-sections (Zhuang et al., 2022b). Different from the

133   simplification in the eigenfrequency prediction method, the size of tree crown here is determined based

134   on real tree data, corresponding to the frontal area distribution of the tree crown (Fig. 3(a)). The model

135   divides the tree beam into a set of segments and calculates the tree motion using linear modal analysis.

136   Specifically, the tree deformation is decomposed into a set of vibration modes so that the total

137   displacement is the combined contribution of each mode. According to preliminary research performed

138 by Sellier et al. (2008) and Pivato et al. (2014), the contribution of the first vibration model is far ahead

139 of the other modes for trees with a slender shape. Thus, only the first vibration mode and the

140 corresponding eigenfrequency are utilized in this study. The modeling of air blast pressure accounts for

141 the wind-tree relative motion and large tree deflection by regarding the beam velocity and geometric

142 nonlinearities resulting from the inclination of beam segments relative to the wind direction (θ_i) (Fig.

143 3(b)). With respect to the large tree deflection, we also introduce the impact of eccentric gravity into the

144 model, which significantly contributes during the interaction with a powerful air blast. The gravity and

145 wind load acting on each segment can be easily calculated based on the predetermined diameter and

146 frontal area distribution (Fig. 3(a)). Considering that trees often fall in the direction of landslide motion

147 and have little time to sway, the maximum response of the tree is assumed to be reached before the

148 damping forces act (Bartelt et al., 2018). Only the undamped response to a short-duration blast is

149 considered. The tree motion equations and the expression of air blast force are as follows:

$$m\frac{\partial^2 y}{\partial t^2} + ky = \int_0^h F_i \phi \, \mathrm{d}s + \int_0^h G_i \phi \, \mathrm{d}s \tag{8}$$

$$F_i = 0.5\rho C_\mathrm{d} A_\mathrm{f} \left| v\cos\theta_i - \frac{\partial y}{\partial t}\cos\theta_i \right| \left(v\cos\theta_i - \frac{\partial y}{\partial t}\cos\theta_i \right) \cos\theta_i \tag{9}$$

$$G_i = m_i g \cdot \sin\theta_i \cdot \cos\theta_i \tag{10}$$

153 where ϕ, w, $m = \int_0^h \overline{m}\phi^2 \mathrm{d}s$, $k = 4\pi^2 m\omega^2$ are the first mode shape, the first eigenfrequency, modal mass

154 and stiffness, respectively, $\overline{m}$ is the mass distribution, y is the associated generalized displacement, F_i

155 and G_i are the air blast loading and eccentric beam gravity act on the ith segment, h is the tree height, C_d

156 is the drag efficient, A_f is the frontal area, ρ and v are the density and velocity of the air blast, respectively.

157 Our model is applicable of calculating the scenarios for both full-height and part-height air blasts.

158  In this study, the air blast velocity is expressed as a sine wave impulse with a short duration time t_0:

$$v = v_{\max}\sqrt{\sin\varpi t} \tag{11}$$

160   where v_{max} is the maximum velocity of the landslide-induced air blast and ϖ can be regarded as the

161   circular frequency of the wind force $\varpi = \pi / t_0$ (wind force is related to the square of its velocity).

162   The mechanical response of trees subject to an air blast is deduced by introducing the calculated

163   wind velocity from Eq. 11 into the tree motion model (Eqs. 8-9), and subsequently solving the equations

164   using the central finite-difference scheme. The validity of this tree motion model has been checked by

165   Pivato et al. (2014) and Zhuang et al. (2022), and thus the validation process is not involved here.
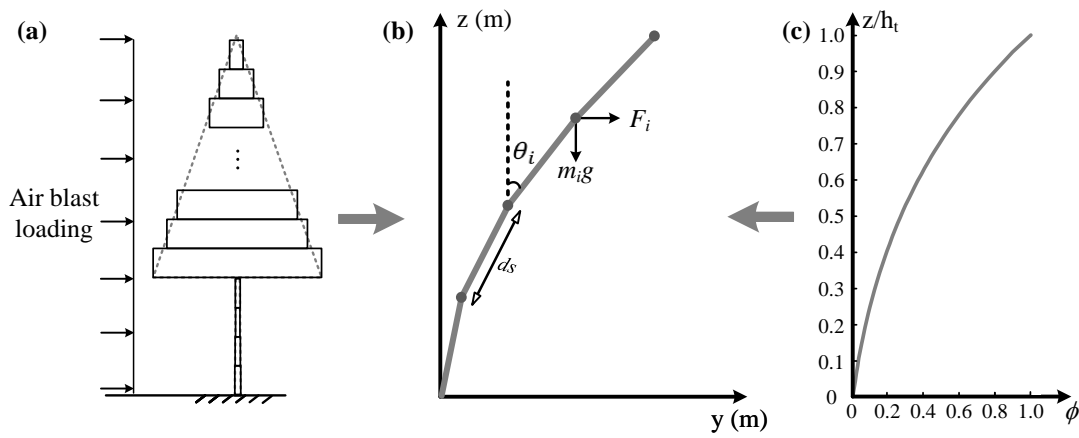
166
167   **Fig. 3** a-b Modeling the tree as a multi-degree-of-freedom flexible beam to calculate the dynamic
168   response of trees submitted a powerful air blast. c The first mode shape of the beam helps to model the
169   tree deformation.

170   *2.3 Tree breakage*

171   Two failure modes commonly caused by air blasts are involved in the work: bending and overturning

172   (Gardiner et al., 2000).

173   For the case of tree bending, trees are considered to break when the maximum bending stress σ_{max}

174   exceeds a critical value σ_{crit} :

$$\sigma_{max} = \left[\frac{M(t,z) \cdot d(z)/2}{I(z)} \right]_{max} \geq \sigma_{crit} \tag{12}$$

176   where σ_{crit} is the bending strength of the tree, which depends highly on the material property. $M(t,z)$ is

177   the bending moment, and its value is calculated at each time step all along the beam:

$$M(t,z) = EI(z) \frac{d\theta}{ds} \tag{13}$$

179   where $\dfrac{\mathrm{d}\theta}{\mathrm{d}s}$ represents the local beam curvature and θ is the angle between the beam segment with the

180   vertical direction.

181   For the tree overturning case, trees are regarded to break at the basement when the air blast-induced

182   moment reaches the anchorage resistance (M_{crit}):

183 $$M_{base}(t) \geq M_{crit}$$ (14)

184   where $M_{base}(t)$ is the moment at tree base calculated at each time step, and the anchorage resistance M_{crit}

185   is often determined based on in-situ tests (e.g. tree pulling tests).

186   **3. Application**

187   To demonstrate the power of air blasts and how they damage trees, we consider the problem proposed

188   by Bartelt et al. (2018): a landslide-induced air blast enters a spruce forest at high speed (maximum

189   velocity of 20 m/s). The short-duration air blast lasts a few seconds with a frequency ϖ . Trees in the

190   forest have a height between 25 and 30 m, which is also the height of the air blast. The sliding mass has

191   stopped before reaching the forest and only the air blast loads on the trees.

192   **Table 1** Model parameters used in the numerical simulations of the tree response. Parameters are derived
193   from data contained in Kantola and Mäkelä (2004) and Bartelt et al. (2018).

Height h(m)	Crown height l(m)	Crown width w(m)	Diameter at trunk base D(m)	Wood density ρ_2 (kg/m³)	Branch mass m(kg)	Drag coefficient C_d
27	18	5	0.4	480	540	0.4

194   Using the measured biomass parameters presented in Table 1, we set the total crown mass of a single

195   tree to be 540 kg. The tree crown is assumed to be a cone with a length of 18 m ($\frac{2}{3}h$) and a width of 5

196   m. The wood density is 480 kg/m³ and the elastic modulus is 10 GPa. Measurements of root anchorage

197   stiffness (K) are very rare and in-situ tests on spruce performed by Neild and Wood (1999) show a value

198   variation of 80-1200 kN·m. This value range indicates a large variation in K depending on the growth

199   conditions, and the values of 100-1200 kN·m are applied in the prediction of eigenfrequency and

200 vibration mode in this study.

201 The eigenfrequency ranging from 0.13 Hz (K=100 kN·m) to 0.32 Hz (K=1200 kN·m) is calculated

202 based on the above parameters (Fig. 4). The modeled results are in high agreement with measurements

203 performed by Jonsson et al. (2006) (0.16-0.30 Hz), indicating the validity of our proposed eigenfrequency

204 prediction method. Although the tree eigenfrequency varies significantly with the anchorage stiffness, all

205 the calculated values are less than 0.5 Hz. The same order of magnitude between tree eigenfrequency

206 and air blast frequency necessitates a further investigation on the possible impact of resonance. The

207 dynamic magnification effect caused by impulse loading can greatly amplify the static stress state,

208 making the trees easier to be damage.

209
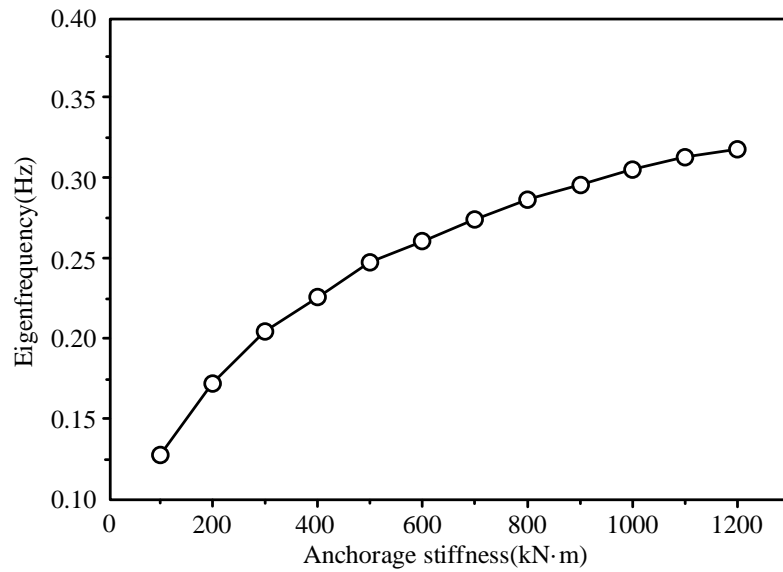
210 **Fig. 4** Eigenfrequency of trees corresponding to different anchorage stiffness.

211 To investigate the impact of dynamic magnification, we performed simulations for all the scenarios

212 using the tree eigenfrequency of 0.26 Hz (K=600 kN·m) and the associated vibration mode. A

213 magnification factor D is defined to describe this effect:

$$D = \frac{u_{d,max}(\beta)}{u_{sta}} = \frac{u_{d,max}(\beta)}{\int_0^h F_{s,max}\phi ds / k} = \frac{u_{d,max}(\beta)}{\int_0^h \rho C_d A_f v_{max}^2 \phi ds / k} \tag{15}$$

214

215 where $u_{d,max}$ and u_{sta} are the maximum displacement subject to dynamic load and static load, respectively,

216     $F_{s,max}$ is the static wind force corresponding to the maximum air blast velocity and $\beta = \dfrac{\varpi}{\omega}$ is the ratio

217   between the air blast frequency (ϖ) and the eigenfrequency of the tree (ω). Notably, the air blast is a

218   multi-medium fluid that contains numerous dusts, showing a higher density than air. Measurements and

219   numerical modeling performed by Swiss researchers (Feistl et al., 2015) suggest $\rho = 5\text{kg}/\text{m}^3$. In this

220   scenario u_{sta} is calculated to be 9.8 m.
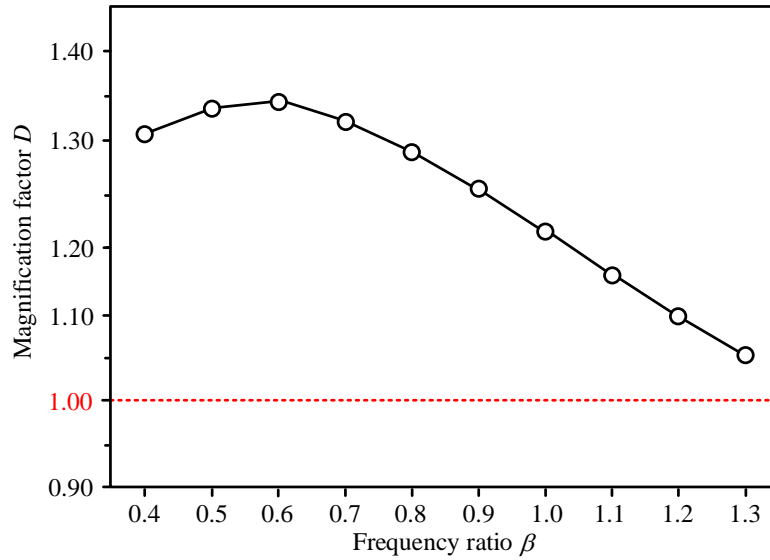
222   **Fig. 5** Magnification factor with various frequency ratio.

223   Figure 5 shows the impact of air blast frequency on the dynamic magnification effect. A parabola

224   relationship is identified between the magnification factor and the frequency ratio. Consider first an

225   impulse air blast lasting 1.6 s ($\beta = 1.2$). The air blast frequency is higher than that of the tree, implying

226   the maximum displacement reaches after the loading time. The modeled maximum dynamic deformation

227     $u_{d,max}$ reaches 10.7 m, and the magnification factor is 1.09. In this case, the magnification effect of tree

228   deformation seems not significant because of the large tree deflection and short-duration loading, and

229   the modeled result is similar to the static stress state. For a longer air blast duration of 3.2 s ($\beta = 0.6$), we

230   find $D=1.34$, a high value. The maximum tree deformation reaches during the air blast loading. In such

231   a scenario, an air blast travelling at 20 m/s can exert similar destruction as a long-duration wind moves

232   at 25 m/s. The dynamic magnification effect significantly increases the tree displacement and thus causes

233   such a phenomenon. Measurements of air blast duration reported by Russian and Swiss researchers

234   (Grigoryan et al., 1982; Sukhanov, 1982) are within this range, lasting only a few seconds. Although the

235   large tree deflection decreases the wind loading, the impulse air blast load is prone to damage the trees

236   because of the dynamic magnification effect.

237   Additional simulations were performed on the air blast induced-tree breakage. The impulse air blast

238   is assumed to have a maximum velocity of 20 m/s and a duration of 3.2 s. For this case, numerical results

239   demonstrate the maximum bending stress and moment of 35 Mpa and 192 kN·m, respectively. The

240   maximum bending stress reaches at 9 m height ($1/3h$), and the maximum bending moment is identified

241   at the tree base. In natural forest areas, the bending strength σ_{crit} and anchorage resistance M_{crit} are highly

242   variable, depending on tree species, soil characteristics and temperatures, etc. Measurements conducted

243   by Peltola et al. (2000) and Lundström et al. (2007) indicate that the bending stress to destroy mature

244   trees needs to exceed a value of 30 MPa while mature spruces with a height of 20-40 m have an anchorage

245   resistance reaches up to 100-400 kN·m. For the case performed in this study, the forest is likely to damage

246   in both bending and overturning failure modes. Reliable values of critical parameters are needed during

247   the assessment of tree destruction, and this will improve the prediction accuracy of the likely failure

248   mode.

249   A further application was performed on the 2008 Wenjia valley avalanche-induced air blast in

250   Sichuan, China (Fig. 6a). This large avalanche has a volume of over $40 \times 10^6 \, \text{m}^3$ and generated a powerful

251   air blast. According to our previous investigations and numerical modeling (Zhuang et al. 2019), the air

252   blast-damaged trees are mostly tall spruce concentrated near the turning points of the valley (Fig. 6 b-c).

253   The simulated air blast velocity at turning points reaches 30 m/s (point A) and 35 m/s (point B),

254   respectively. Using the spruce-related parameters indicated in Table 1 and an assumed air blast duration

255   of 3.2 s (a long duration for large avalanches), the maximum displacement of spruces is calculated to be

256   18.5 m and 22.2 m at points A and B, respectively. In this case, the maximum bending stress of trees at

257   two turning points could reach 51 Mpa and 57 Mpa, respectively, significantly larger than the bending

258   strength suggested by Peltola et al. (2000) (36 Mpa). Therefore, bending failure of tall spruces was widely

259   identified in situ.
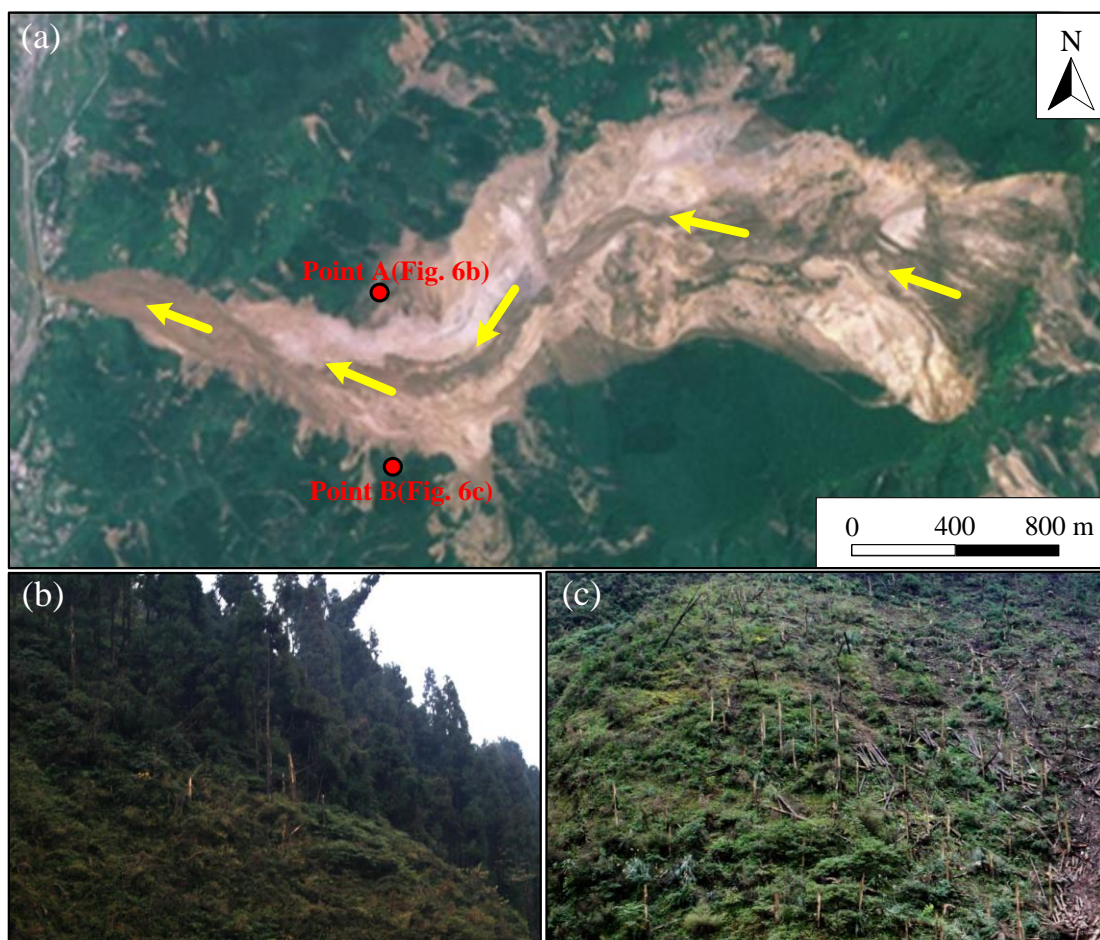
261   **Fig. 6** Wenjia valley avalanche-induced air blast (according to Zhuang et al. 2019). a Overview of the

262   Wenjia valley avalanche. b-c Trees damaged by the generated air blast.

263   **4. Discussion**

264   Risk assessment and disaster mitigation of landslide-induced air blasts are hot issues in mountainous

265   regions. Developing a simple but applicable relationship between air blast pressure and tree failure is of

266   great utility for scientists to quantify the air blast power. Compared with existing models, one significant

267   improvement of our model is to model the tree as a flexible beam with variable cross-section and involve

268   the impact of anchorage. This improvement allows the tree to move as its natural vibration mode rather

269   than a hypothetical trajectory (e.g. rotate around the tree base as a rigid body (Bartelt et al., 2018)).

270   Moreover, the variable cross-section makes the modeling of tree bending failures more realistic. We can

271   simulate the failure position of trees subjected to a powerful air blast. For the existing model with a

272   constant diameter (Feistl et al., 2015), the rigidity EI is constant along the beam, and the maximum

273   bending stress is always identified at the tree base. This failure characteristic cannot match the actual

274   situation well.

275   Our proposed model accounts for the impacts of large tree deflection: eccentric gravity and

276   modeling of air blast force regarding the wind-tree relative motion and geometric nonlinearities. To

277   investigate the impact of these factors and confirm the necessity of considering large deflection, a

278   comparative analysis is needed to make readers have a better understand. Therefore, we designed a

279   comparative analysis by simplifying the tree motion model of Eq. 8 without involving the impact of large

280   tree deflection. The simplified model is similar to that proposed by Bartelt et al. (2018):

281
$$m\frac{\partial^2 y}{\partial t^2} + ky = \int_0^h 0.5\rho C_d A_f v_{max}^2 \phi ds \cdot \sin \varpi t = \int_0^h F_{s,max} \phi ds \cdot \sin \varpi t \tag{16}$$

282   The displacement at the tree top can be written as:

283
$$\begin{cases} u(t) = \dfrac{\int_0^h F_{s,max} \phi ds}{k} \dfrac{1}{1-\beta^2}(\sin \varpi t - \beta \sin \omega t) & 0 \le t \le t_0 \\ u(t) = \dfrac{u'(t_0)}{\omega}\sin \omega(t-t_0) + u(t_0)\cos \omega(t-t_0) & t > t_0 \end{cases} \tag{17}$$

284   The maximum deformation occurs during the loading time when $\beta \le 1$, and after the loading time

285   when $\beta > 1$. The magnification factor D for both scenarios can be expressed as:

$$\begin{cases} D = \dfrac{1}{1-\beta^2}[\sin(\dfrac{2\pi\beta}{\beta+1}) - \beta\sin\dfrac{2\pi}{\beta+1}] & \beta \leq 1 \\ D = \dfrac{2\beta}{\beta^2-1}\cos\dfrac{\pi}{2\beta} & \beta > 1 \end{cases} \tag{18}$$
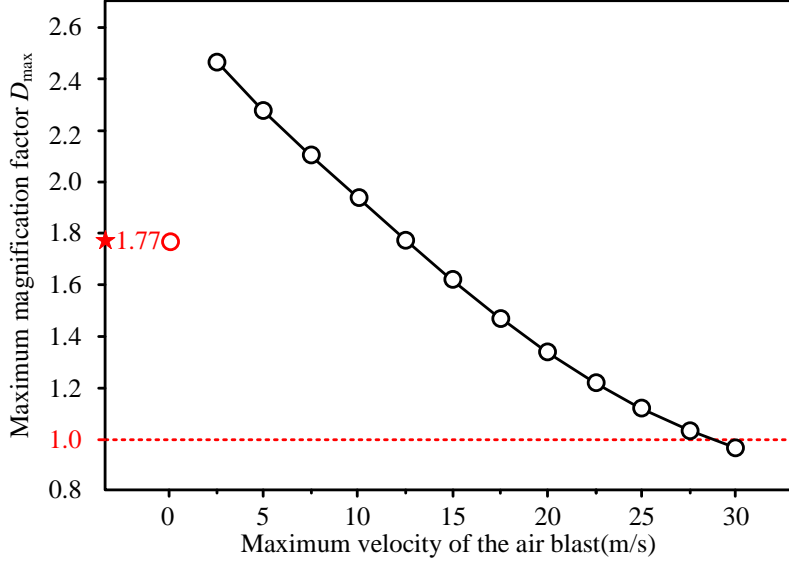
Fig. 7 Impact of large tree deflection on the maximum magnification factor D_{max}. The red star represents the D_{max} calculated from Eq. 18. The red circle represents the D_{max} corresponding to the scenario with a very low air blast velocity (maximum velocity of 0.1m/s) and the eccentric gravity is not considered.

Figure 7 presents the impact of large tree deflection on the magnification effect. We first perform the simulation using the proposed model without regarding the impact of large tree deflection. A very low air blast velocity (maximum velocity of 0.1m/s) is performed and the eccentric gravity is not considered. The D_{max} value of 1.77 is identified in the scenario, which is consistent with the analytical solution from Eq. 18. The tree deformation is small with such a weak air blast loading, and the comparison result verifies the validity of our proposed model. Further calculations with higher air blast velocities show different results. In the cases of a low air blast velocity, the eccentric gravity contributes a lot to the tree deformation, causing a rather large magnification factor (>2). However, D_{max} greatly decreases with the increase of wind velocity. For a high air blast velocity, the dynamic response and eccentric gravity amplify the tree deflection, but the inclination of the trees to the wind direction significantly reduces the air blast loading. This special mechanism was rarely considered during the

302   previous assessment of landslide-induced air blasts. We suggest that the modeled tree deformation

303   subjected to a powerful air blast might be overestimated without considering large tree deflection,

304   although this simplified model of Eq. 18 has the advantage of rapid assessment for air blast pressure. The

305   impact of large tree deflection should be accounted for when using forest destruction to quantify the air

306   blast danger.

307   The dynamic response of trees subject to a landslide-induced air blast is a complex problem,

308   depending heavily on the biometric characteristics of trees. Some biomass variations can be represented

309   by the parameters in the proposed model. For example, for the leafless trees, air blasts pass through the

310   tree crown and only act on the branches, causing a smaller wind load. A reduction of drag efficient C_d is

311   needed in such a condition. Single trees in the impact region of air blasts are subject to a larger loading

312   than trees in dense forest stands, where tree crowns tend to be narrower and form a shielding effect. We

313   can make a reduction in the frontal area A_f to simulate this mechanism. Furthermore, although much

314   effort has been paid to the biometric and mechanical characteristics of tree crowns and trunks, less

315   information is available about the anchorage stiffness and resistance. The root anchorage properties

316   significantly influence the tree eigenfrequency and the likely failure mode. A reliable measurement value

317   of tree bending strength and anchorage resistance is of utility to improve the accuracy of tree failure

318   prediction and clarify which failure mode is prone to occur. Overall, biomass-related parameters selected

319   to estimate the air blast pressure are recommended to be determined based on in-situ investigations. In

320   the future, more measurements need to be conducted on the anchorage properties of trees. Regional

321   databases for biometric and mechanical properties of trees are worthwhile to be established. This would

322   help provide reliable parameters for the air blast risk assessment.

323   In this study, the tree is modeled as a variable cross-section that is hinged at ground level using

324   elastic support. Root anchorage is complex and sensitive to many factors such as soil mechanical

325   properties, soil water content and root morphology, and we acknowledge that it is difficult to establish a

326   model that accounts for all the factors that affect the anchorage. Most importantly, we developed a simple

327   but practical model that could simulate the dynamic response of trees subject to a powerful air blast and

328   their two possible failure modes. Bartelt and his colleagues (Bartetl et al., 2018) have developed a

329   dynamic model named RAMMS, which could efficiently model the entire movement process of

330   ice/rock/snow avalanches and the associated air blasts. It is anticipated that the combination of our

331   proposed tree model and the RAMMS dynamic model could help the risk assessment of potential air

332   blasts through modeling the air blast impact region and forest destruction.

333   **Conclusions**

334   Air blasts are short-duration impulses and can intensity the potential destruction far beyond the sliding

335   mass. Trees destruction in-situ can provide valuable data to quantify the air blast danger and make us

336   better understand its force of destruction. In this study, we developed a framework for the forest

337   destruction assessment subject to a powerful air blast, including the eigenfrequency prediction method,

338   tree motion equations and breakage conditions. The tree is modeled as a flexible variable cross-section

339   beam hinged at ground using elastic support. The impacts of root anchorage and large tree deflection are

340   regarded during the dynamic response analysis. The framework also involved two failure modes (bending

341   and overturning) and the corresponding failure criteria so that the risk of forest damage could be assessed.

342   Using the proposed framework, we assumed conditions to investigate the air blast power. Modeling

343   results demonstrate that although the anchorage properties significantly influence the tree eigenfrequency,

344   the latter is always in the same order as air blast frequency. The associated dynamic magnification effect

345   amplifies the tree deformation and thus makes the tree damage easier. In the scenario with a similar

frequency between air blasts and trees, an air blast travelling at 20 m/s causes a similar force of

destruction as a long-duration wind load moves at 25 m/s. Notably, this magnification effect caused by

the dynamic response and eccentric gravity is significant in the cases of low wind velocity, while the

large tree deflection caused by strong air blast loading would weaken this effect. Furthermore, bending

and overturning are two likely failure modes for trees subject to a powerful air blast, but exactly what

kind of failure will occur for a specific forest depends heavily on the properties of both trees and soil. A

case application was further performed on the 2008 Wenjia valley avalanche-induced air blast in China,

checking the validity of our proposed model. In the future, more measurements should be conducted on

biometric and mechanical properties of trees, and a regional parameter database is worthwhile to be

established. This would greatly improve the prediction accuracy of tree damage and air blast pressure.

Data availability

No data sets were used in this article.

Copyright statement

All the photos/figures are created by authors and there is no need to add a copyright statement or credit.

Author contribution

Yu Zhuang did the numerical work and wrote the manuscript with contributions from all co-authors.

Aiguo Xing and Perry Bartelt designed the work and modified the manuscript. Bilal Muhammad

evaluated the results and proposed various improvements that were incorporated. Zhaowei Ding helped

with the eigenfrequency prediction model.

Competing interest

The authors declare that they have no known competing financial interests or personal relationships that

could have appeared to influence the work reported in this paper.

Acknowledgments

This study was supported by the National Natural Science Foundation of China (No. 41977215).

References

Adams, J.: Earthquake-dammed lakes in New Zealand, Geology, 9, 215-219, 1881.

Bartelt, P., and Stöckli, V.: The influence of tree and branch fracture, overturning and debris entrainment on snow avalanche flow, Annals of Glaciology, 32, 209-216, 2001.

Bartelt, P., Buser, O., Vera Valero, C., and Bühler, Y.: Configurational energy and the formation of mixed flowing/powder snow and ice avalanches, Annals of Glaciology, 57(71), 179-188, 2016.

Bartelt, P., Bebi, P., Feistl, T., Buser, O., and Caviezel, A.: Dynamic magnification factors for tree blow-down by powder snow avalanche air blasts, Natural Hazards Earth System Sciences, 18, 759-764, 2018.

Bartelt, P., Christen, M., Bühler, Y., and Buser, O.: Thermomechanical modelling of rock avalanches with debris, ice and snow entrainment, Numerical Methods in Geotechnical Engineering IX, Taylor & Francis Group, London, pp 1047-1054, 2018.

Caviezel, A., Margreth, S., Ivanova, K., Sovilla, B., and Bartelt, P.: Powder snow impact of tall vibrating structures, Eccomas Proceedia Compdyn, 5318-5330, 2021.

Feistl, T., Bebi, P., Christen, M., Margreth, S., Diefenbach, L., and Bartelt, P.: Forest damage and snow avalanche flow regime, Natural Hazards and Earth System Sciences, 15, 1275-1288, 2015.

Fujita, K., Inoue, H., Izumi, T., Yamaguchi, S., Sadakane, A., Sunako, S., Nishimura, K., Immerzeel, W. W., Shea, J. M., Kayastha, R. B., Sawagaki, T., Breashears, D. F., Yagi, H., and Sakai, A.: Anomalous winter-snow-amplified earthquake-induced disaster of the 2015 Langtang avalanche in Nepal, Natural Hazards Earth System Sciences, 17, 749-764, 2017.

390   Gardiner, B., Peltola, H., and Kellomäki, S.: Comparison of two models for predicting the critical wind

391   speeds required to damage coniferous trees, Ecological Modelling, 129, 1-23, 2000.

392   Grigoryan, S., Urubayev, N., and Nekrasov, I.: Experimental investigation of an avalanche air blast, Data

393   Glaciology Student, 44, 87-93, 1982.

394   Jonsson, M. J., Foetzki, A., Kalberer, M., Lundström, T., Ammann, W., and Stöckli, V.: Root-soil rotation

395   stiffness of norway spruce (Picea abies (L.) Karst) growing on subalpine forested slopes, Plant Soil,

396   285, 267-277, 2006.

397   Johnson, B. C., and Campbell, C. S.: Long-runout landslides are among the most spectacular and

398   catastrophic geologic processes, Geophysical Research Letters, 44(12), 12091-12097, 2017.

399   Kantola, A., and Mäkelä, A.: Crown development in Norway spruce [Picea abies(L.) Karst.], Trees, 18,

400   408-421, 2004.

401   Kargel JS, et al. (2016) Geomorphic and geologic controls of geohazards induced by Nepal's 2015

402   Gorkha earthquake. Science, 351, aac8353.

403   Keshmiri, A., Wu, N., and Wang, Q.: Free Vibration Analysis of a Nonlinearly Tapered Cone Beam by

404   Adomian Decomposition Method, International Journal of Structural Stability and Dynamics, 18(7),

405   1850101, 2018.

406   Lundström, T., Jonsson, M. J., and Kalberer, M. The root-soil system of Norway spruce subjected to

407   turning moment: resistance as a function of rotation, Plant Soil, 300, 35-49, 2007.

408   Mocica, G.: Special Functions Problems, Bucharest: Didactic and Pedagogic Publishing House, 1988.

409   Neild, A. S., and Wood, C. J.: Estimating stem and root-anchorage flexibility in trees, Tree Physiology,

410   19, 141-151, 1999.

411   Nicoletti, P. G., and Sorriso-Valvo, M.: Geomorphic controls of the shape and mobility of rock

412   avalanches, Geological Society of America Bulletin, 103, 1365-1373, 1991.

413   Nicoletti, P. G., Parise, M., and Miccadei, E. The Scanno rock avalanche (Abruzzi, south-central Italy),

414   Bollettino della Società geologica italiana, 112, 523-535, 1993.

415   Nicoll, B. C., Gardiner, B. A., Rayner, B., Peace, A. J.: Anchorage of coniferous trees in relation to

416   species, soil type, and rooting depth, Canadian Journal of Forest Research, 36, 1871-1883, 2006.

417   Penna, I. M., Hermanns, R. L., Nicolet, P., Morken, O. A., and Jaboyedoff, M.: Airblasts caused by large

418   slope collapses, Geological Society of America Bulletin, 133, 939-948, 2021.

419   Peltola, H., Kellomäki, S., Väisänen, H., and Ikonen, V.: A mechanistic model for assessing the risk of

420   wind and snow damage to single trees and stands of scots pine, norway spruce, and birch, Canadian

421   Journal of Forest Research, 29, 647-661, 1999.

422   Peltola, H., Kellomäki, S., Hassinen, A., and Granander, M.: Mechanical stability of Scots pine, Norway

423   spruce and birch: an analysis of tree-pulling experiments in Finland, Forest Ecology and

424   Management, 135, 143-153, 2000.

425   Pivato, D., Dupont, S., and Brunet, Y.: A simple tree swaying model for forest motion in windstorm

426   conditions, Trees, 28, 281-293, 2014.

427   Sellier, D., Brunet, Y., and Fourcaud, T.: A numerical model of tree aerodynamic response to a turbulent

428   airflow, Forestry, 81(3), 279-297, 2008.

429   Shugar, DH. et al.: A massive rock and ice avalanche caused the 2021 disaster at Chamoli, Indian

430   Himalaya, Science, 373(6552), 300-306, 2021.

431   Šilhán, K.: Tree ring evidence of slope movements preceding catastrophic landslides, Landslides, 17,

432   615-626, 2020.

433 Sukhanov, G.: The mechanism of avalanche air blast formation as derived from field measurements, Data

434   Glaciology Student, 44, 94-98, 1982.

435 Yin, Y. P., and Xing, A. G.: Aerodynamic modeling of the yigong gigantic rock slide-debris avalanche,

436   Tibet, China. Bulletin of Engineering Geology and the Environment, 71, 149-160, 2012.

437 Yin, Y. P.: Vertical acceleration effect on landsides triggered by the Wenchuan earthquake, China.

438   Environmental Earth Sciences, 71, 4703-4714, 2014.

439 Zhang, K. Q., Wang, L. Q., Dai, Z. W., Huang, B. L., and Zhang, Z. H: Evolution trend of the

440   Huangyanwo rock mass under the action of reservoir water fluctuation. Natural Hazards, 113, 1583-

441   1600, 2022.

442 Zhuang, Y., Xu, Q., and Xing, A. G.: Numerical investigation of the air blast generated by the Wenjia

443   valley rock avalanche in Mianzhu, Sichuan, China, Landslides, 16, 2499-2508, 2019.

444 Zhuang, Y., Xu, Q., Xing, A. G., Bilal, M., Gnyawali, K. R. (2022) Catastrophic air blasts triggered by

445   large ice/rock avalanches, Landslides, 2022. Doi: 10.1007/s10346-022-01967-8.

446 Zhuang, Y., Xing, A. G., Jiang, Y. H., Sun, Q., Yan, J. K., and Zhang, Y. B.: Typhoon, rainfall and trees

447   jointly cause landslides in coastal regions, Engineering Geology, 298, 106561, 2022b.